Processing and Application of Ceramics 14 [1] (2020) 25–31
https://doi.org/10.2298/

Properties of MWCNTs added Si_3N_4 composites processed from oxidized silicon nitride powders

Awais Qadir[1], Katalin Balazsi[2], Csaba Balazsi[2], Michal Ivor[3], Jan Dusza[1,3,*]

[1]*Doctoral School of Materials Sciences and Technologies, Óbuda University, Bécsi ut. 96/b, 1034 Budapest, Hungary*
[2]*Institute of Technical Physics and Materials Science, Centre for Energy Research, 1121 Budapest, Konkoly-Thege str 29-33, Hungary*
[3]*Institute of Materials Research, Slovak Academy of Sciences, Watsonova 47, 04001 Košice, Slovak Republic*

Received 13 September 2019; Received in revised form 1 December 2019; Accepted 24 January 2020

Abstract

Si_3N_4/3 wt.% multi-walled carbon nanotubes (MWCNTs) composites were prepared from oxidized α-Si_3N_4 powders and sintering additives by hot isostatic pressing (HIP). The Si_3N_4 powders were oxidized at 1000 °C in ambient air environment for 10 and 20 h and the powder mixture was sintered at 1700 °C for 3 h under the pressure of 20 MPa in nitrogen. The relationship between oxidation, microstructure, tribology and mechanical properties was studied. The dispersion of MWCNTs was not optimal, as they were found mainly in the form of bundles between the β-Si_3N_4 grains. Neither Si_2N_2O nor other oxide phase were observed after the sintering. This was probably caused by the presence of MWCNTs at the grain boundaries of the Si_3N_4 grains causing reduction of oxide phases. The density, hardness, bending strengths and friction coefficient of the composites increased with the oxidation time of the Si_3N_4 powder.

Keywords: *α-Si_3N_4, oxidation, carbon nanotubes, hot isostatic pressing (HIP), composites*

I. Introduction

Silicon nitride (Si_3N_4) has excellent physical, chemical and mechanical properties including hardness, strength and fracture toughness at room and elevated temperatures which make them suitable for use in many structural applications [1]. The microstructure of these ceramics is strongly dependent on their processing route and determines their complex properties at room and high temperatures [2,3].

In the past, different silicon nitride-based composites have been developed with fine-grained matrix and *ex situ* or *in situ* introduced elongated β-Si_3N_4 grains with significantly improved fracture toughness [4–7]. On the other hand, silicon nitride-based composites have been developed using different second phase ceramics, such as microsized and nanosized SiC with the aim to improve their high temperature properties [3,8–10]. Another type of the second phase, carbon nanotubes (CNTs) with very high stiffness, strengths and excellent thermal and electrical conductivity, offer a new way to develop Si_3N_4-based composites with improved mechanical, tribological, thermal and functional properties [11–15]. A number of works have demonstrated that processing of Si_3N_4 composite with the addition of CNTs has a potential to improve selected properties of the composite.

Balazsi *et al.* [16] used spark plasma sintering (SPS) and hot isostatic pressing (HIP) for preparation of carbon nanotube reinforced silicon nitride composites with preserved CNTs. The processing route had significant influence on the microstructure development and mechanical properties of the composites. They reported higher strength for Si_3N_4/CNTs composites in comparison to the monolithic silicon nitrides at the similar level of porosity for both systems.

Pasupuleti *et al.* [17] prepared 1 wt.% CNTs reinforced Si_3N_4 composites by hot pressing (HP) technique. They showed the slight decrease of Vicker's hardness and increase of the fracture toughness with addition of CNTs. The toughness increased due to the toughen-

* Corresponding author: tel: +421 55 7922 489,
e-mail: *duszaj@yahoo.com*

ing mechanism such as crack-bridging and pulling-out effect of CNTs. Moreover, R-curve behaviour increased with the addition of CNTs which enhanced the toughening behaviour of the composite.

Tatami *et al.* [18] developed the electrically conductive silicon nitride composites with the addition of CNTs for high-performance static-electricity-free bearings for aerospace and other high-performance components. It was observed that CNTs have tendency to react with SiO_2 or Si_3N_4 and O_2 to form CO, CO_2 and SiC at higher temperature and disappear from the composite. To avoid the disappearance of CNTs, the densification was done at lower temperature using TiO_2, AlN, Y_2O_3 and Al_2O_3 as sintering additives. In this way, the CNTs reinforced silicon nitride composite with high electrical and mechanical properties was prepared.

Belmonte *et al.* [19] recently produced a new, highly electrically conducting silicon nitride-based nanocomposites with nitrogen-doped multi-walled carbon nanotubes (MWCNTs). The composites have excellent electrical conductivity with values above 2150 S/m connected with the enhanced electro-wetting mechanism, shifting the Si_3N_4 particle rearrangement temperature to a lower value than in the case of nanocomposites containing pure MWCNTs. Moreover, the efficiently dispersed nanotubes from bundles by oxidizing treatment improved the nanotubes-matrix interphase which resulted in an improved mechanical performance.

According to these reports, the homogeneous distribution of CNTs in the silicon nitride matrix is a big challenge. The inhomogeneous distribution and agglomeration tendency of CNTs significantly downgrade the properties of final composites. Several methods have been employed to improve the dispersion and densification like highly efficient ultrasonic agitation [12]. In the case of milling process, further optimization is needed to improve the dispersion of CNTs. The milling time, milling conditions and the type of the mill have great influence on the morphology and microstructure of the starting powders for homogeneous dispersion reinforcement [20,21].

The aim of this investigation is to study the influence of the oxidization of α-Si_3N_4 starting powders on the microstructure, mechanical and tribological properties of Si_3N_4/MWCNT composites.

II. Experimental details

2.1. Materials preparation

Three forms of the starting α-Si_3N_4 powder (Ube, SN-ESP) were used in this investigation: i) as-received α-Si_3N_4 powder (un-oxidized) used as a reference (SN-CNT/0), ii) oxidized α-Si_3N_4 powder at 1000 °C for 10 h in ambient air environment (SN-CNT/10) and iii) oxidized α-Si_3N_4 powder at 1000 °C for 20 h in ambient air environment (SN-CNT/20).

Each batch with 90 wt.% of the α-Si_3N_4 powder (un-oxidized and oxidized for 10 and 20 h) was milled separately with 4 wt.% of Al_2O_3 (Alcoa, A16), 6 wt.% of Y_2O_3 (H.C. Starck, grade C) (Table 1) as sintering additives and polyethylene glycol (PEG) surfactants dispersed in ethanol using high efficient attrition mill (Union Process, type 01-HD/HDDM) equipped with zirconia agitator delta discs and zirconia grinding media (diameter of 1 mm) in a 750 cm^3 zirconia tank. This milling process was performed with high rotation speed 4000 rpm for 4 h. The 3 wt.% MWCNTs was added in the mixture and mixed for 30 min at the 600 rpm in the attrition mill. The multi-walled carbon nanotubes (MWCNTs) were produced by catalytic-chemical vapour deposition (CCVD) method [22]. The low rpm was used to avoid the damaging of MWCNTs in the powder. A similar powder preparation process was used in previous works [23,24]. The drying and sieving process with 150 μm mesh number were done after the milling process. Each batch of powders was subjected to the dry pressing consolidation process under 200 MPa pressure to produce green samples with the dimensions of 3.5 × 5 × 50 mm. The heat treatment of green samples was done at 400 °C in the muffle furnace to eliminate the PEG prior to the sintering process. After the heat treatment of the green samples, the samples were sintered at 1700 °C and 20 MPa in nitrogen (N_2) gas environment for 3 h as a holding time with the heating rate of 25 °C/min, similar as in our previous work [23].

2.2. Materials characterization

Phase compositions of the powders and sintered materials were analysed by X-ray diffractometer (XRD, Bruker AXS D8) with Cu-Kα radiation. Morphology,

Table 1. Summarized data about starting composition

	SN-CNT/0	SN-CNT/10	SN-CNT/20
Oxidation time [h]	0	10	20
Oxidation temperature [°C]	0	1000	1000
α-Si_3N_4 [wt.%]	90	90	90
MWCNTs [wt.%]	3	3	3
Al_2O_3 [wt.%]	4	4	4
Y_2O_3 [wt.%]	6	6	6
Specific surface area [m^2/g]	6.6	6.6	6.6
A-phase content [wt.%]	>95	>95	>95
Crystallinity [wt.%]	>99.5	>99.5	>99.5

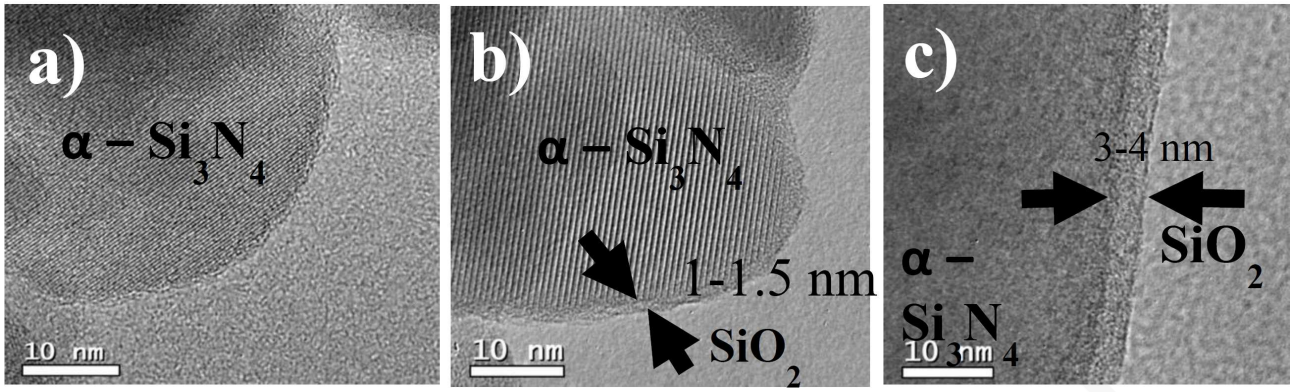

Figure 1. High resolution electron microscopy (HREM) images of Si_3N_4 powders without SiO_2 layers (a) and with SiO_2 layers formed after the oxidation of powders during 10 h (b) and 20 h (c), based on [23]

shape and homogeneity of the powders and MWCNTs were examined by scanning electron microscopy (SEM, LEO 1540 XB). Energy dispersive X-ray spectroscopy (EDS) was carried out for the qualitative analysis of the base powders (un-oxidized and oxidized Si_3N_4 powders) for the quantification of elemental compositions. Transmission electron microscopy (TEM, Philips CM-20) with accelerating voltage of 200 kV was carried out for the microstructural characterization of the oxidized powders. High resolution transmission electron microscopy (HRTEM, JEOL3010) with accelerating voltage of 300 kV was used for the nanostructural analysis of the oxidized powders and sintered samples. The density of the sintered materials was measured by the Archimedes method. The hardness was tested by Vicker's indentation with 10 N load applied for 10 s in each case. Elastic modulus and flexural strength (3- and 4-points bending strength) of the sintered samples using specimens with the size 3×4×45 mm were measured by bending tests on a tensile/loading machine (INSTRON-1112).

Tribology measurements were carried out on equipment UMT 3 (Bruker) using the reciprocating ball-on-plate sliding technique. The wear behaviour of the experimental materials was studied in dry sliding in air. The tribological partner was a highly polished (roughness $Ra < 0.10\,\mu m$ according to ISO 3290) Si_3N_4 ball with 6.35 mm diameter. The normal applied load was 13.5 N that corresponds to a Hertzian pressure of 2.0 GPa, the sliding speed was 10 mm/s and the sliding distance was 720 m. The experiments were realized at room temperature at the relative humidity of 40 ± 5%. The material losses (volume of the wear tracks) due to the wear were measured by a high precision confocal microscope PLuneox 3D Optical Profiler by SENSOFAR, and then specific wear rates (W) were calculated in terms of the volume loss (V) per distance (L) and applied load (F_p) according to the equation:

$$W = \frac{V}{L \cdot F_p} \tag{1}$$

III. Results and discussion

3.1. Microstructural characterization

Microstructural characterization and phase analysis of the precursor Si_3N_4 powders confirmed the presence of α-Si_3N_4 phase before and after oxidation (Figs. 1, 2 and 3). The detected crystalline and amorphous phases correspond with the α-Si_3N_4 and SiO_2, respectively. The amorphous SiO_2 phase was formed as the result of reaction between Si_3N_4 and O_2 during the oxidation. The thickness of the observed amorphous SiO_2 phase was approximately 1.5 nm and 4 nm with the oxidation time of 10 and 20 h, respectively (Fig. 1).

The X-ray diffractograms of the starting α-Si_3N_4 powders with 3 wt.% MWCNTs before and after oxidation are shown in Fig. 2. No phase transformation from α to β-Si_3N_4 was observed before and after oxidation of the starting powders. The XRD peaks correspond mainly to α-Si_3N_4 according to the JCPDS PDF-01-076-1407 before sintering. There is no peak representing the CNT. MWCNTs were supposed to have a peak at the $2\theta = 26.228$ position according to the (JCP2: 01-075-162), but the value was below detection limit

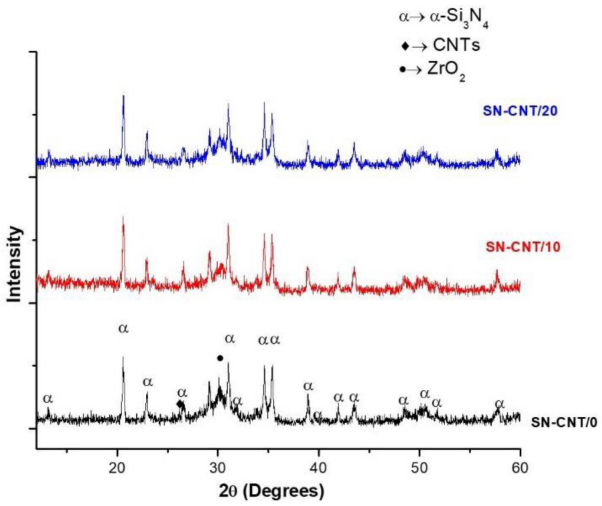

Figure 2. X-ray diffractograms of starting powder mixtures with un-oxidized (SN-CNT/0) and with 10 h oxidized (SN-CNT/10) and 20 h oxidized (SN-CNT/20) Si_3N_4 powders

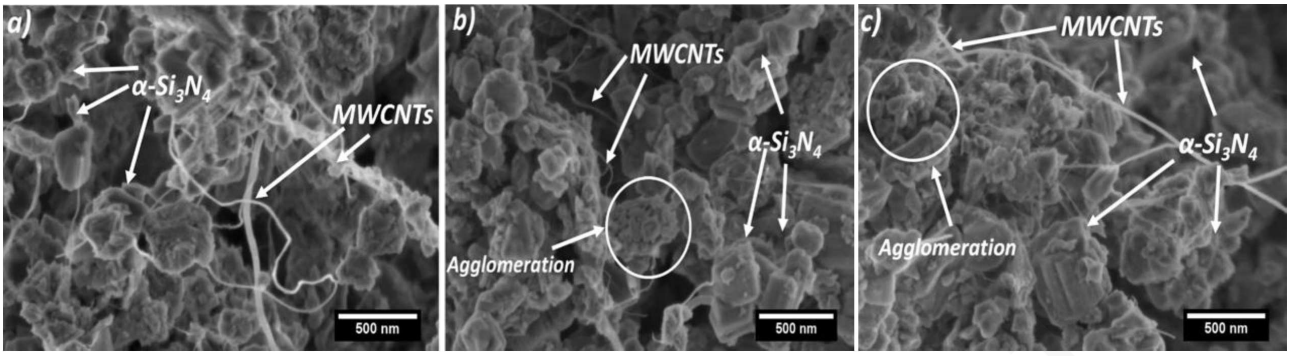

Figure 3. SEM images of the starting powders mixtures with 3 wt.% of MWCNTs after the attrition milling and the CNTs network is among the α grains of Si_3N_4 powder: a) SN-CNT/0, b) SN-CNT/10 and c) SN-CNT/20

of XRD. The presence of MWCNTs was confirmed by structural observations (Fig. 3). The zirconia contamination originated from the grinding media (JCPDS PDF-00-83-0944).

The higher atomic percent of oxygen was detected by EDS after oxidation for 10 and 20 h at 1000 °C which can be explained by the formation of amorphous SiO_2 films on the surface of α-Si_3N_4 powders illustrated in Fig. 1. In the case of the sample prepared with 20 h oxidized α-Si_3N_4 powder, five times higher atomic percent of oxygen was detected than that of the sample prepared with un-oxidized powder [23]. In this current work, no structural peaks of any oxygen-containing phase (including SiO_2) were detected by XRD after oxidation. Moreover, the oxidation of the starting powders increased the apparent density (Table 2) which might have the influence on the mechanical properties. Carbon might cause a mass loss in the sintered samples during sintering because of the reduction of SiO_2:

$$3\,SiO_2(l) + 6\,C + 2\,N_2 \longleftrightarrow Si_3N_4 + 6\,CO \qquad (2)$$

More likely, the SiO_2 reacted to a limited extent with MWCNTs during sintering, but CO was formed in only small amount.

Table 2. Apparent density (ρ_{ap}) and relative densities (ρ_r) of the sintered composites

	SN-CNT/0	SN-CNT/10	SN-CNT/20
ρ_{ap} [g/cm^3]	3.161	3.199	3.235
ρ_r [%TD]	93.4	94.5	95.6

Although MWCNTs were not detected in XRD measurements, the incorporation of MWCNTs in the starting powders was clearly visible (Fig. 3a). SEM images show that there is no significant damage of MWCNTs fibres and their length and diameter are up to 8 to 10 μm and 10 to 30 nm, respectively (Fig. 3). The particle size of silicon nitride was reduced from 50–500 nm to 30–300 nm after milling. The agglomerations of small particles of the powders might be mixture of sintering additives and zirconia (Fig. 3). The grouping and clustering of MWCNTs were also observed in some areas of the starting powders (Fig. 3).

XRD diffractograms revealed the complete α to β transformation of Si_3N_4 after sintering at 1700 °C for 3 h holding time in nitrogen environment (Fig. 4). These transformations have been observed in several works [25,26]. Two main phases β-Si_3N_4 (JCPDS PDF-00-33-1160) and ZrO_2 (JCPDS PDF-00-83-0944) were identified in the XRD diffractograms of all sintered composites (Fig. 4). Surprisingly, Si_2N_2O was not found in any of the sintered sample. Si_2N_2O was supposed to be formed during sintering at high temperature because of the presence of oxygen content in starting powders. Previously, Si_2N_2O was formed by the oxidization of the starting powders and its effects on the mechanical properties were observed [23]. The reason might be the reaction occurring between the surface oxygen on the silicon nitride and carbon nanotubes. CO and CO_2 might be formed as the result of reaction between oxygen and carbon nanotubes at higher temperature during sintering which reduced the amount of carbon in the sintered samples. The release of carbon by the oxidation in the composite has been reported by other researchers as well [18,27]. No peak of carbon was found in the XRD diffractograms, but the MWCNTs can be seen clearly in SEM images of the fractured surfaces (Fig. 5).

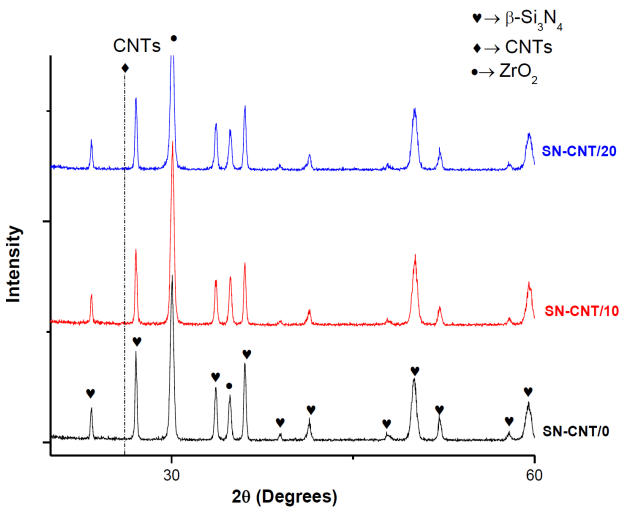

Figure 4. XRD patterns of the composites after sintering at 1700 °C for 3 h of un-oxidized (SN-CNT/0), 10 h oxidized (SN-CNT/10) and 20 h oxidized (SN-CNT/20) Si_3N_4 powders

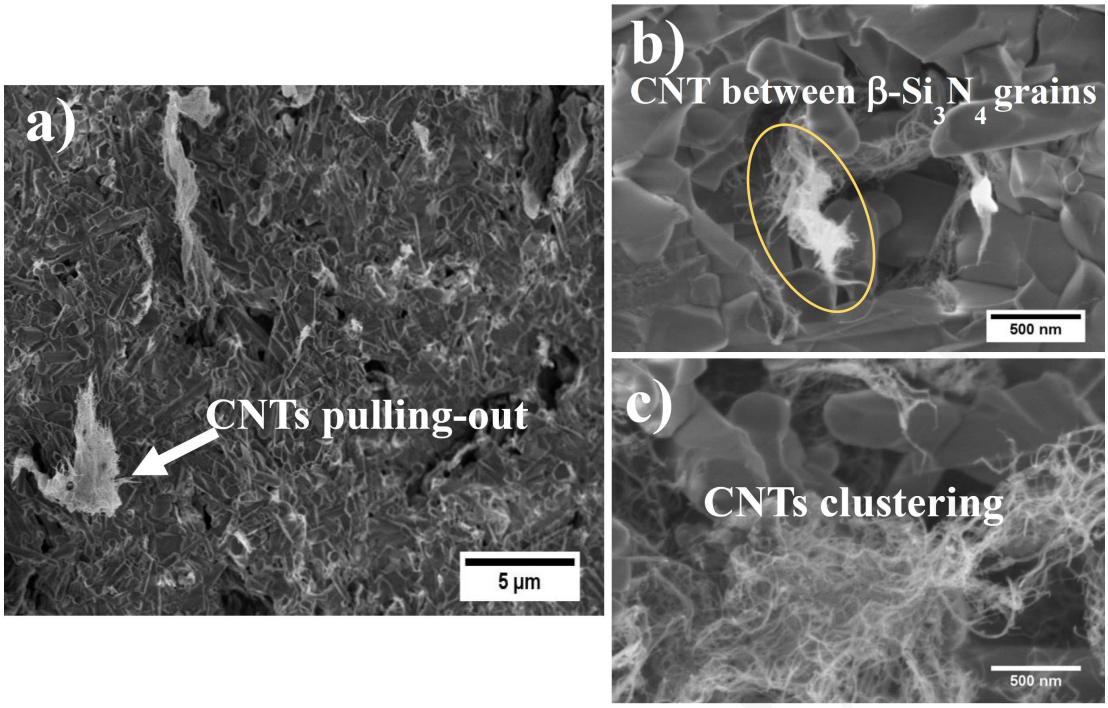

Figure 5. Fracture characteristics of the investigated composites with characteristic fracture surface for all systems. Overview of the fracture surface of SN-CNT/20 where pulling-out of MWCNTs can be seen (a). The agglomerates of MWCNTs are present in SN-CNT/10 (b) and agglomerates/clusters of MWCNTs are seen in un-oxidized SN-CNT/0 sample (c)

3.2. Mechanical properties

As illustrated in Fig. 6, the hardness of the investigated composites increased with increasing oxidation time of the Si_3N_4 powder. The maximum hardness was measured in the case of the samples containing 20 h oxidized Si_3N_4 powder and the lowest hardness value was measured in the reference sample (SN-CNT/0). The low hardness values in comparison to the monolithic ceramics prepared using the same oxidized Si_3N_4 powders (~14 GPa) can be explained with the low density and relatively high porosity present in the composites after processing.

Similar tendency was found for bending strength values. The oxidation time of the powders positively influences the density of the investigated systems, which has a positive influence not only on the hardness but also on the bending strength values.

The 4-points bending strength of the samples SN-CNT/0 (un-oxidized), SN-CNT/10 and SN-CNT/20 were 249.5, 263.25 and 296.6 MPa, respectively (Fig. 7). Strength increase of 16% of the SN-CNT/20 (20 h oxidized) with increase in apparent density of 2% was observed in comparison to the SN-CNT/0 (un-oxidized sample). Similar tendency was found in the case of 3-point bending strength with the strength values of

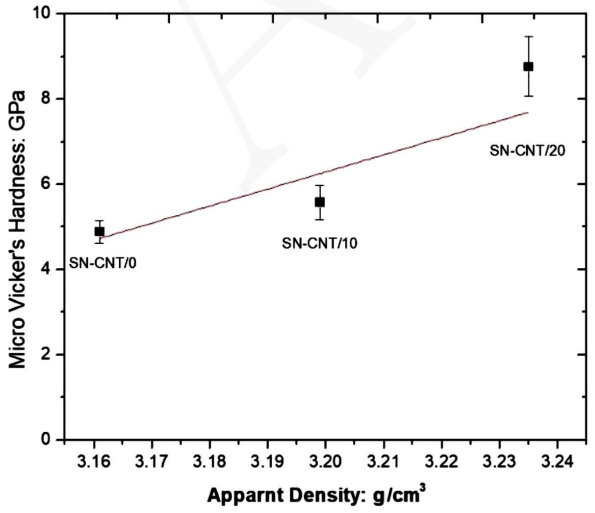

Figure 6. Mechanical properties of the sintered composites - the influence of apparent density on the hardness of the investigated systems

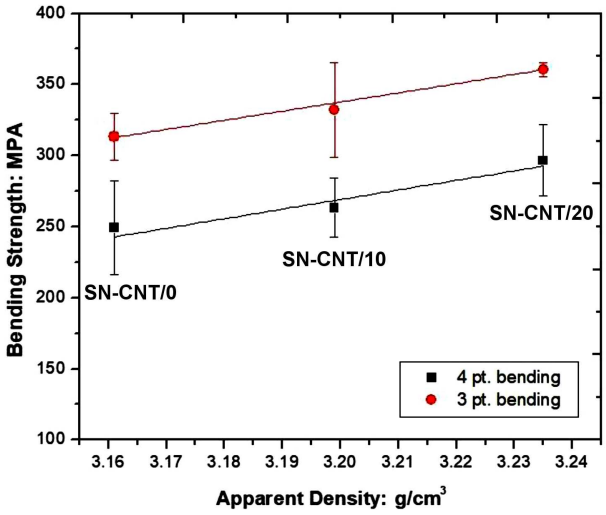

Figure 7. Influence of the apparent density on the 3- and 4-points bending strengths of the investigated systems

the samples SN-CNT/0 (un-oxidized), SN-CNT/10 and SN-CNT/20 being 313.25, 332.0 and 360.4 MPa, respectively (Fig. 7). Relatively low bending strength was caused by the present porosity and agglomeration/clusters of MWCNTs in the composites, but also with the MWCNTs being located between the grains of β-Si_3N_4 and weakening the bonding between the grains. The higher strength value in the case of 3-points bending mode can be explained by the lower effective volume in the case of 3-points bending mode in comparison to the 4-points mode and with the lower probability of the presence of strength decreasing defects close to the tensile surface of the samples. Balazsi *et al.* [12] reported the similar relation between density and strength. They reported the strength is attributed to the density of the composite.

3.3. *Fractography of the fracture surfaces*

Fractographic analyses have been realized on the fracture surfaces of the specimens after the bending strength test (Fig. 5). Macrofractography revealed that in all cases the fracture surfaces were typical for low strength materials, without the characteristic areas such as fracture origin, mist, mirror and hackle [28].

Microfractography shows no significant differences in the microstructure and fracture of the investigated composites. The microstructure of these systems consists of β-Si_3N_4 grains with the average grain diameter of approximately 0.35 μm and with the average length of 1.1 μm similar to the grain dimension for the systems prepared without CNTs addition. The composites contain pores with the size approximately from 1 to 10 μm often filled with agglomerates of CNTs. The composite with longer oxidation of starting powders contains less porosity. The fracture character is mixed inter and intra-granular often with bundles of pulled-out CNTs with length up to 20 μm.

The wear test revealed that in all cases friction after short initial stage (in order of meters) was rather stable and reproducible. There are no significant differences in the friction coefficients of the investigated composites

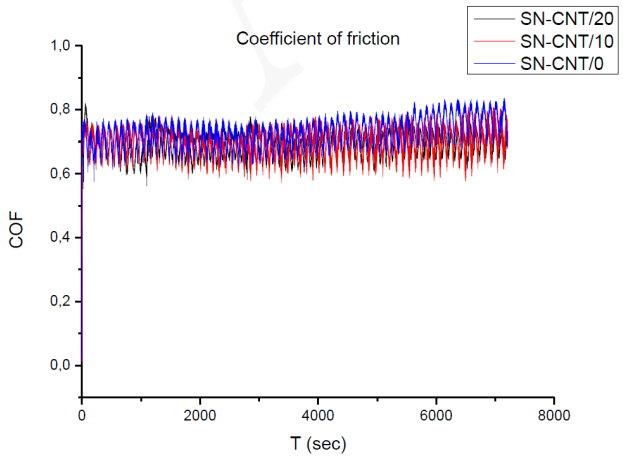

Figure 8. Coefficient of friction (COF) vs. sliding time of the composites

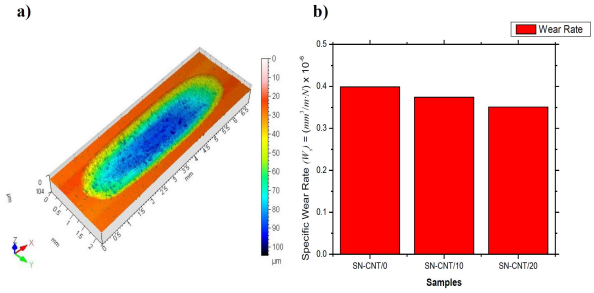

Figure 9. Tribological behaviour of the composites: confocal microscopy image of wear track (a) and wear volume of the investigated composites (b)

over the test running distance giving values between 0.6 and 0.7 along the sliding distance (Fig. 8). This result is in a very good agreement with our previous work [29] where we found similar or even higher coefficient of friction for Si_3N_4/MWCNTs composites with the COF starting to decrease only when the MWCNT content reached 5 wt.%. The confocal microscopy (Fig. 9a) illustrates the wear track of the sample. The maximum wear happened in the central part of the wear track. The specific wear rate was slightly decreased with the oxidation time (Fig. 9b). Similarly, as in the case of hardness and bending strength the increased density has a positive influence on the wear resistance of the investigated composites and with the increasing density the wear volume decreased.

Microscopic observations of the worn surfaces of the composites revealed no significant pulled-out CNTs and development of so-called transferred film, which could significantly lower the friction coefficient. It seems that the present of 3 wt.% CNTs in the investigated composites was not enough effective in creating the transferred film.

IV. Conclusions

Si_3N_4/MWCNTs composites with 3 wt.% of multi-walled carbon nanotubes were prepared from oxidized α-Si_3N_4 powders and sintering additives by hot isostatic pressing. The influence of the oxidation of silicon nitride powders on the microstructure development, mechanical and tribological properties was studied. The main results are the followings:

- Composites with un-damaged carbon nanotubes were prepared with increased density from 3.16 to 3.24 g/cm^3 with the increased time of oxidation;
- The microstructure of the composites consists of β-Si_3N_4 grains, porosity and MWCNTs often in the form of CNTs bundles. The fracture character of the systems is mixed inter and intra-granular often with pulled-out CNTs bundles;
- The mechanical and tribological properties increased with the increasing oxidation time of the composites. Significant improvement can be obtained after optimization of the processing route - homogenization of CNTs and densification of the powder mixture.

Acknowledgement: A. Qadir thanks for the Stipendium Hungaricum Scholarship Program. K. Balázsi, C. Balázsi and J. Dusza acknowledge the support given by the Hungarian National Research Development and Innovation Office for the funding of FLAG-ERA "Multifunctional Ceramic/Graphene Coatings for New Emerging Applications". Thanks to V. Varga, S. Gurban, L. Illés, Dr. Zs. E. Horvath and Dr. H.R. Ben Zine from MTA EK for sample preparation, sintering, performing SEM, XRD and bending strength measurements, respectively.

References

1. G. Petzow, M. Herrmann, "Silicon nitride ceramics", pp. 47–167 in *High Performance Non-Oxide Ceramics II*, M. Jansen, Ed. Berlin, Heidelberg: Springer Berlin Heidelberg, 2002.
2. S. Hampshire, "Silicon nitride ceramics – Review of structure, processing and properties", *J. Achiev. Mater. Manuf. Eng.*, **24** [1] (2007) 43–50.
3. H. Klemm, "Silicon nitride for high-temperature applications", *J. Am. Ceram. Soc.*, **93** [6] (2010) 1501–1522.
4. P. Šajgalík, J. Dusza, M.J. Hoffmann, "Relationship between microstructure toughening mechanisms and fracture toughness of reinforced silicon nitride ceramics", *J. Am. Ceram. Soc.*, **78** [10] (1995) 2619–2624
5. J. Dusza, P. Šajgalík, "Mechanical properties of Si_3N_4 + β-Si_3N_4 whisker reinforced ceramics", *J. Eur. Ceram. Soc.*, **9** (1992) 9–17.
6. J.J. Kruzic, R.L. Satet, M.J. Hoffmann, R.M. Cannon, R.O. Ritchie, "The utility of R-curves for understanding fracture toughness-strength relations in bridging ceramics", *J. Am. Ceram. Soc.*, **91** [6] (2008) 1986–1994.
7. T. Fett, S. Funfschilling, M. Hoffmann, R. Oberacker, H. Jelitto, G. Schneider, "R-curve determination for the initial stage of crack extension in Si_3N_4", *J. Am. Ceram. Soc.*, **91** (2008) 3638–3642.
8. K. Niihara, "New design concept of structural ceramics – Ceramic nanocomposites", *J. Jpn. Ceram. Soc.*, **99** [10] (1991) 974–982.
9. A. Rendtel, H. Hubner, M. Herrmann, C. Schubert, "Silicon nitride/silicon carbide nanocomposite materials: II, Hotstrength, creep, and oxidation resistance", *J. Am. Ceram. Soc.*, **81** [5] (1998) 1109–1120.
10. P. Šajgalík, M. Hnatko, F. Lofaj, P. Hvizdos, J. Dusza, P. Warbichler, F. Hofer, R. Riedel, E. Lecomte, M.J. Hoffmann, "SiC/Si_3N_4 nano/micro-composites- processing, RT and HT mechanical properties", *J. Eur. Ceram. Soc.*, **20** [4] (2000) 453–462.
11. M. Matsuoka, S. Yoshio, T. Yamakawa, J. Tatami, T. Wakihara, K. Komeya, T. Meguro, "Development of CNT-Si_3N_4 composites with high strength and electrical conductivity by adding HfO_2", *Trans. Mater. Res. Soc. Jpn.*, **37** [1] (2012) 11–14.
12. C. Balázsi, B. Fényi, N. Hegman, Z. Kövér, F. Wéber, Z. Vértesy, Z. Kónya, I. Kiricsi, L.P. Biró, P. Arató, "Development of CNT/Si_3N_4 composites with improved mechanical and electrical properties", *Compos. Part B Eng.*, **37** [6] (2006) 418–424.
13. J. Gonzalez-Julian, J. Schneider, P. Miranzo, M.I. Osendi, M. Belmonte, "Enhanced tribological performance of silicon nitride-based materials by adding carbon nanotubes", *J. Am. Ceram. Soc.*, **94** [8] (2011) 2542–2548.
14. A. Kovalčíková, Cs. Balázsi, J. Dusza, O. Tapasztó, "Mechanical properties and electrical conductivity in a carbon nanotube reinforced silicon nitride composite", *Ceram. Int.*, **38** [1] (2012) 527–533.
15. P. Ge, K. Sun, A. Li, G. Pingji, "Improving the electrical and microwave absorbing properties of Si_3N_4 ceramics with carbon nanotube fibers", *Ceram. Int.*, **44** [3] (2018) 2727–2731.
16. C. Balázsi, Z. Shen, Z. Konya, Zs. Kasztovszky, F. Weber, Z. Vertesy, L.P. Biro, I. Kiricsi, P. Arato, "Processing of carbon nanotube reinforced silicon nitride composites by spark plasma sintering", *Composites Sci. Technol.*, **65** (2005) 727–733.
17. S. Pasupuleti, R. Peddetti, S. Santhanam, K.P. Jen, Z.N. Wing, M. Hecht, J.P. Halloran, "Toughening behavior in a carbon nanotube reinforced silicon nitride composite", *Mater. Sci. Eng. A*, **491** [1] (2008) 224–229.
18. J. Tatami, T. Katashima, K. Komeya, T. Meguro, T. Wakihara, "Electrically conductive CNT-dispersed silicon nitride ceramics", *J. Am. Ceram. Soc.*, **88** [10] (2005) 2889–2893.
19. M. Belmonte, S.M. Vega-Díaz, A. Morelos-Gómez, P. Miranzo, M.I. Osendi, M. Terrones, "Nitrogen-doped-CNTs/Si_3N_4 nanocomposites with high electrical conductivity", *J. Eur. Ceram. Soc.*, **34** [5] (2014) 1097–1104.
20. M. Matsuoka, J. Tatami, T. Wakihara, K. Komeya, T. Meguro, "Improvement of strength of carbon nanotube-dispersed Si_3N_4 ceramics by bead milling and adding lower-temperature sintering aids", *J. Asian Ceram. Soc.*, **2** [3] (2014) 199–203.
21. O. Tapasztó, C. Balázsi, "The effect of milling time on the sintering kinetics of Si_3N_4 based nanocomposites", *Ceram. Int.*, **36** [7] (2010) 2247–2251.
22. Z. Kónya, I. Vesselenyi, K. Niesz, A. Kukovecz, A. Demortier, A. Fonseca, J. Delhalle, Z. Mekhalif, J.B. Nagy, A.A. Koós, Z. Osvath, "Large scale production of short functionalized carbon nanotubes", *Chem. Phys. Lett.*, **360** [5] (2002) 429–435.
23. A. Qadir, Z. Fogarassy, Z.E. Horváth, K. Balazsi, C. Balazsi, "Effect of the oxidization of Si_3N_4 powder on the microstructural and mechanical properties of hot isostatic pressed silicon nitride", *Ceram. Int.*, **44** [12] (2018) 14601–14609.
24. C. Balazsi, "Silicon nitride composites with different nanocarbon additives", *J. Korean Ceram. Soc.*, **49** [4] (2012) 352–362.
25. D. Bučevac, S.B. Bošković, B. Matović, "Kinetics of the α-β phase transformation in seeded Si_3N_4 ceramics", *Sci. Sinter.*, **40** [3] (2008) 263–270.
26. L. Wang, T.-Y. Tien, I.-W. Chen, "Formation of β-silicon nitride crystals from (Si,Al,Mg,Y)(O,N) liquid: I, Phase, composition, and shape evolutions", *J. Am. Ceram. Soc.*, **86** [9] (2003) 1578–1585.
27. C. Balázsi, F. Wéber, P. Arató, "Investigation of C/Si_3N_4 nanocomposites", *Mater. Werkst.*, **34** [4] (2003) 332–337.
28. J. Dusza, M. Steen, "Fractography and fracture mechanics property assessment of advanced structural ceramics", *Int. Mater. Rev.*, **44** [5] (1999) 165–216.
29. P. Hvizdoš, V. Puchý, A. Duszová, J. Dusza, C. Balázsi, "Tribological and electrical properties of ceramic matrix composites with carbon nanotubes", *Ceram. Int.*, **38** [7] (2012) 5669–5676.